applied sciences

MDPI

Article

Effect of Laser Remelting on Wear Behavior of HVOF-Sprayed FeCrCoNiTiAl$_{0.6}$ High Entropy Alloy Coating

Lijia Chen [1], Dingyong He [2], Bing Han [1], Zhen Guo [1], Li Zhang [1], Longxing Lu [1], Xu Wang [2], Zhen Tan [2] and Zheng Zhou [2,*]

[1] Institute of Intelligent Manufacturing, Guangdong Academy of Sciences, Guangdong Key Laboratory of Modern Control Technology, Guangzhou 510070, China; lj.chen@giim.ac.cn (L.C.); b.han@giim.ac.cn (B.H.); z.guo@giim.ac.cn (Z.G.); l.zhang@giim.ac.cn (L.Z.); lx.luo@giim.ac.cn (L.L.)

[2] Faculty of Materials and Manufacturing, Beijing University of Technology, Beijing 100124, China; dyhe@bjut.edu.cn (D.H.); wangxu1203@emails.bjut.edu.cn (X.W.); zhen.tan@bjut.edu.cn (Z.T.)

* Correspondence: zhouzhengbjut@bjut.edu.cn; Tel.: +86-010-67392168

Received: 12 September 2020; Accepted: 13 October 2020; Published: 16 October 2020

Abstract: In this study, a laser remelting process was applied to the FeCrCoNiTiAl$_{0.6}$ high entropy alloy coating in order to improve the density and the surface quality of the coating. The coating was fabricated by high-velocity-oxygen-fuel (HVOF) technology. The microstructure and phase composition of the coating were investigated by scanning electron microscopy (SEM), energy dispersive X-ray spectrometer (EDS), X-ray diffractometer (XRD) and confocal scanning laser microscope (CSLM). Moreover, the wear behavior of the coating was evaluated by use of a ball-on-disc test. The coating was denser after laser remelting treatment by eliminating the previous lamellar structure. The microstructure of the laser-remelted coating exhibits two body-centered cubic (BCC) phases, which is different from the HVOF coating. In addition, aluminum oxide formed during laser remelting. Different from the wear mechanism of the HVOF coating, which comprised abrasion and fatigue, the major wear of the laser remelted coating was abrasion.

Keywords: high entropy alloy; coating; laser remelting; microstructure; friction behavior

1. Introduction

High entropy alloys (HEAs) have received significant research focus in recent years since they were proposed [1–6]. Due to their unique compositions, HEAs exhibit some interesting properties, such as high strength, outstanding fracture toughness, good fatigue resistance and high hardness at elevated temperatures [7–17]. Thermal spray technology is a process in which the spraying powder is heated or melted by a focused thermal energy. During the process, the powder is accelerated and deposited onto the substrate surface to form the coating. High-velocity-oxygen-fuel (HVOF) technology is a commonly used thermal spray technology that has a lower particle temperature and higher flight particle velocity. The low temperature can reduce the oxidation of particles during melting while the high velocity can produce dense coating after high speed impact on the matrix. HEAs can be deposited on substrates to form protective coatings by thermal spraying techniques and the coatings retain the microstructure and excellent properties [18–22]. It is worth noting that wear behavior is a very important property amongst the mechanical properties in applications. For example, the wear behavior of molds, tools and structural components cannot be neglected in applications. However, there are few studies on the wear behavior of HEA coatings for now. Huang et al. [4] investigated the wear behavior of AlCrFeMo$_{0.5}$NiSiTi and AlCoCrFeMo$_{0.5}$NiSiTi coatings produced by atmospheric plasma spraying. The wear resistance of the coatings was similar to SUJ2 steel, and the hardness of the coatings was

525 HV and 485 HV, respectively. When the coatings were heat-treated for 1 h at 800 °C, the hardness increased to 900 HV and the wear resistance was better than SUJ2 steel and SKD61 steel. Löbel et al. [23] studied the hardness and the wear resistance of AlCoCrFeNiTi HEA coatings produced by HVOF. The hardness of the coating amounted to 730 $HV_{0.1}$, and the coating exhibited outstanding wear resistance in oscillating wear, ball-on-disk and scratch tests. Hsu et al. [3] studied the wear behavior of $NiCo_{0.6}Fe_{0.2}Cr_{1.5}SiAlTi_{0.2}$ HVOF coatings. They found that the wear resistance of the coating was better than SUJ2 steel and SKD61 steel. As an important surface treatment process, laser remelting process is often used to improve the density and bonding strength as wel as to reduce the porosity of coatings. However, thus far, research involving laser remelted HEA coatings is sparse. Cai et al. [24] investigated the effect of laser remelting processing on microstructure and wear behavior of laser clad Ni-Cr-Co-Ti-V high entropy alloy coating. The results showed that the phase composition of the coating remained unchanged and the micro-hardness increased to 900 HV after laser remelting processing. In contrast to the as-clad high-entropy alloy coating, the laser remelted high-entropy alloy coatings had a lower friction coefficient and lower wear mass, and the worn mechanism of as-clad and as-remelted high-entropy alloy coatings showed adhesive wear.

To date, the wear behavior of laser remelted HVOF coatings have been reported rarely. It was reported that the laser remelting process could improve the compactness [25]. Therefore, in the present study, the laser remelting process was used to produce the laser remelted $FeCrCoNiTiAl_{0.6}$ HVOF coating. The microstructure, phase composition and hardness of the coating was analyzed. The wear behavior and the wear mechanism were investigated at room temperature. In order to compared the properties, the as-sprayed HVOF coating was also investigated in this study.

2. Materials and Methods

$FeCrCoNiTiAl_{0.6}$(at.%) high entropy alloy coating which was prepared in the laboratory was used to study the effect of laser remelting processing on microstructure and wear behavior. The coating was prepared by HVOF on ASTM A572 steel substrates. The spraying process, parameter and characterization of the powder and coating was introduced in our former study [26]. In this study, the coating was grinded and cleaned by ethanol before laser remelting. A YLS-6000 fiber laser (IPG Laser GmbH, Burbach, Germany) with a Gaussian energy distribution in the laser-beam was used to remelt the coatings. A multi-pass laser surface remelting with linear scanning was conducted. The parameters are as follows: laser power of 800 W, overlapping ratio of 50%, scanning speed of 12 mm/s, beam diameter of 2.5 mm. In order to prevent oxidation, high-purity argon gas (10 mL/min) Guangzhou yuejia gases Co. Ltd, Guangzhou, China) was used during laser remelting processing. Specimens with dimension of 15 × 15 mm^2 were prepared and preheated to 200 °C before remelting to avoid cracking.

The phase compositions of the HVOF coating and the laser remelted coating were characterized using an Ultima IV X-ray diffractometer with a Cu target (Rigaku corporation, Shibuya Tokyo, Japan). The microstructures of the coatings were studied by scanning electron microscopy (SEM) using TM4000PLUS tabletop microscope from Hitachi Ltd. (Tokyo, Japan), equipped with a Model 550i energy dispersive X-ray spectrometer (EDS, Hitachi Ltd., Tokyo, Japan).

The microhardness of the coatings was measured via a Vickers microhardness tester (Laizhou Huayin Testing Instrument Co., Ltd., Shandong, China). The measurement was conducted in the cross-section of the samples, which were grinded and polished before test with a load of 0.982 N and a dwell time of 15 s.

The wear behavior of the coatings was studied using a MS-T3001 Friction & Wear tester by Lanzhou Huahui Instrument Technology Co., Ltd. (Lanzhou, China) without lubricant in air environment at room temperature. In order to get a condition mainly for abrasion wear, an Al_2O_3 ball with a diameter of 4 mm was used as counter body. A normal load of 5 N, measurement radius of 2.5 mm at a sliding speed of 382 rpm/min and measurement duration of 83 min were used in wear tests. The measurement was conducted on the surface of the coatings, which were ground and polished before the tests.

The friction coefficient of the samples during the tests was recorded automatically. The volume loss of the coating was measured by using a confocal scanning laser microscope (CSLM, LEXT OLS4100, Olympus corporation, Japan). The wear rates were calculated by dividing the volume loss by normal load and sliding distance. The surface and cross-sections of the wear track were investigated by CSLM, SEM and EDS.

3. Results and Discussion

3.1. Microstructure and Phase Composition

The XRD patterns of the $FeCrCoNiTiAl_{0.6}$ HVOF coating and the laser remelted HVOF coating are shown in Figure 1. The HVOF coating exhibits a BCC-type phase. After laser remelting, the coating exhibits two kinds of BCC-type phases. Between the two BCC-type phases, BCC1 phase keeps the same with the HVOF coating and BCC2 phase has a smaller lattice constant. The phase change is mainly attributed to the characteristic of laser remelting process. During the laser remelting process, the HVOF coating was heated to a very high temperature, then cooled down at a high speed (generally 10^5 K/s [27]). However, the solidification rate in this process was much slower than thermal spraying (about 10^7 K/s [28]). In this case, the elements in the coating migrated drastically due to the thermal effect. This resulted in that the single BCC phase changed to two BCC phases. Meanwhile, a small amount of aluminum oxide phase was detected as a result of oxidation behavior.

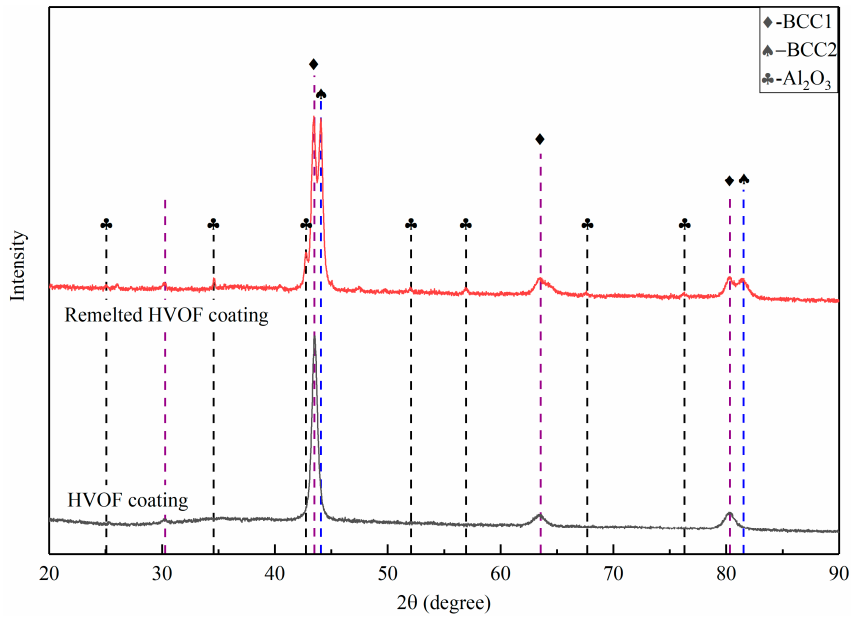

Figure 1. X-ray diffractometer patterns of high-velocity-oxygen-fuel (HVOF) sprayed coating and the laser remelted HVOF coating.

Figure 2 shows the BSE SEM micrographs of the cross-section of the $FeCrCoNiTiAl_{0.6}$ HVOF coating and the laser remelted HVOF coating at low magnification. The HVOF coating consists of plenty of micro-pores resulting from HVOF spray methods. In contrast, the laser remelted HVOF coating is compact and the typical lamellar structure of thermal sprayed HVOF coating disappeared. The pre-existing pores and micro-cracks were remarkably eliminated.

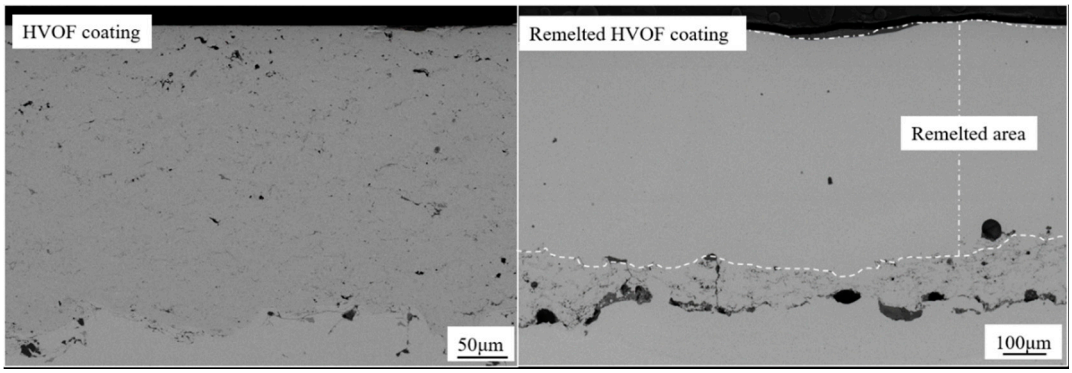

Figure 2. Low-magnification backscattered electron (BSE SEM) images of the cross-section of the coatings.

A high-magnification BSE SEM micrograph of the coatings (Figure 3) shows that some spherical particles of the powder still exist in the HVOF coating and exhibits a dendritic crystal structure. This is because the particles had a high in-flight velocity and the heating time was very short during the HVOF spraying process, resulting in that the particles were not fully melted and retained the characteristics of the HEA powder. Moreover, the spherical particles were reserved and some voids and lamellar structure appeared in the HVOF coating. After laser remelting, the coating was fully crystallized due to the fact that the HVOF coating received vast heat then was fully melted during laser remelting. In this process, the buoyancy effect promoted the gas bubbles to escape from the coating, which favored the elimination of pre-existing pores [29]. It is noted that the microstructure of the laser remelted HVOF coating consists of dendrites of a BCC1 phase (Area 2) and an interdendritic BCC2 phase (Area 1), as wel as oxide (Area 3). The dendritic structure is similar to the structure in HVOF coating. In our former investigation, we found that the HVOF coating consisted of two BCC phases that showed different compositions but exhibited just one set of peaks in XRD analysis due to the similar lattice parameters [26]. During laser remelting, the HVOF coating was fully melted and then cooled down rapidly. In this process, the elements in the coating were distributed differently in dendrite and inter-dendrite regions. The migration of elements led to the phase change, which means that the lattice parameters of the BCC solid solution in HVOF coating changed and the two BCC phases can be differentiated in XRD analysis.

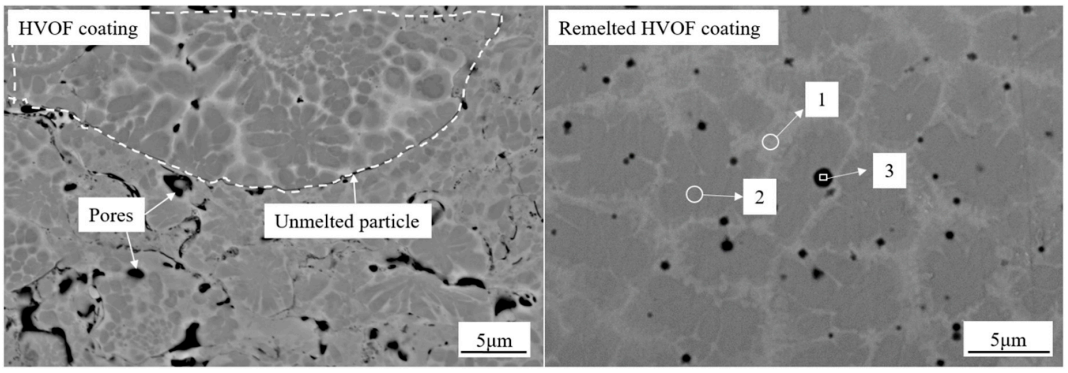

Figure 3. High-magnification BSE SEM micrograph of the cross-section of the coating.

Figure 4 shows the EDS mapping result of the laser remelted HVOF coating. The result shows that all elements can be detected in both dendrite and inter-dendrite regions. However, the elements are distributed non-uniformly, and the dendrite is rich in Al and Ni, while the inter-dendrite is rich in Fe and Cr. In contrast, Cr and Co are distributed more evenly in both regions. The compositions in different areas are investigated by EDS, which are shown in Table 1. A similar microstructure was reported in the literature [23,30].

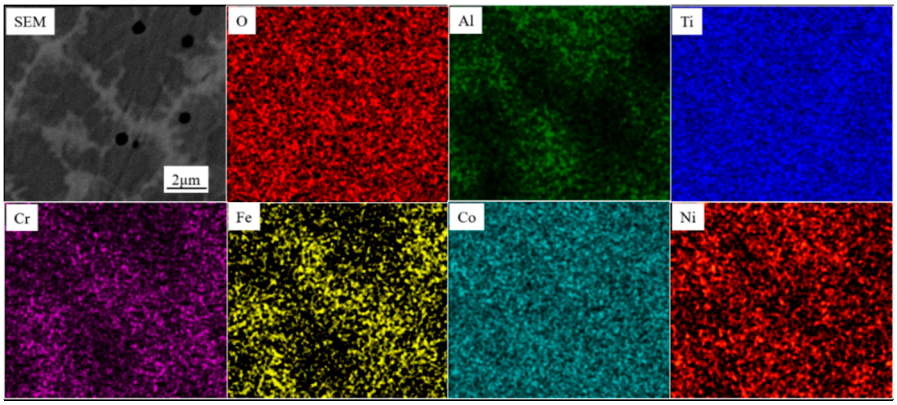

Figure 4. EDS mapping result of the laser remelted HVOF coating.

Table 1. EDS point result of the laser remelted HVOF coating.

Element	O (at.%)	Al (at.%)	Ti (at.%)	Cr (at.%)	Fe (at.%)	Co (at.%)	Ni (at.%)
1	2.74	4.66	13.29	16.13	39.55	12.34	11.29
2	2.67	14.1	12.43	11.35	30.36	14.42	14.66
3	20.95	35.87	9.07	5.39	15.17	6.77	6.79

3.2. Wear Behavior

In this study, ball-on disc test was conducted in order to investigate the wear behavior of the laser remelted $FeCrCoNiTiAl_{0.6}$ HVOF coating. Furthermore, the HVOF coating was also tested for comparison to investigate the effect of laser remelting on wear behavior. Figure 5 shows the friction coefficients of the coatings during test. The values of the friction coefficient are significantly different. The laser remelted HVOF coating has a much lower friction coefficient than HVOF coating. The decrease of the friction coefficient is related to the microstructure of the coatings. The coating is denser and the coefficient is lower. In wear test, the coatings were cut by an Al_2O_3 ball. The elimination of the pores and cracks in laser remelted coating can provide a smooth contact interface, thus reducing the friction coefficient.

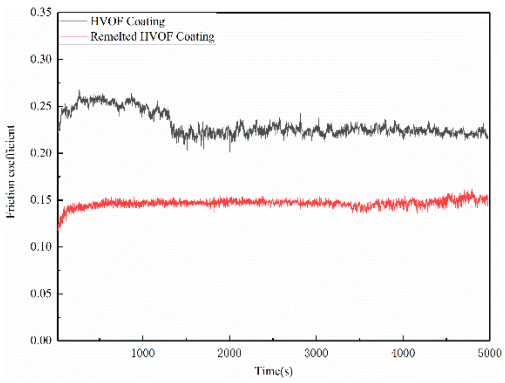

Figure 5. Friction coefficient of the coating.

Figure 6 shows the confocal laser scanning microscopy (CSLM) micrographs in a same magnification of the HVOF coating and the laser remelted HVOF coating. The wear track on the HVOF coating is obviously wider and deeper than the laser remelted HVOF coating. The maximum depth of the wear track is 47.7 μm for HVOF coating and 24.0 μm for laser remelted HVOF coating. The wear rates of the coatings as a function of sliding duration are also shown in Figure 6. The wear rate of the HVOF coating is $W = 4.546 \times 10^{-5}$ $mm^3N^{-1}m^{-1}$, while the wear rate of the laser remelted HVOF coating is $W = 1.375 \times 10^{-5}$ $mm^3N^{-1}m^{-1}$. The wear rate decreased significantly due to the laser

remelting process. As we know, the wear behavior is related to the hardness, the wear rate decreased as the hardness increases. When the HVOF coating was remelted by laser beam, micro-pores and cracks decreased dramatically. The compact microstructure and the precipitate of the Al_2O_3 phase in the coating led to the increase of hardness. In this paper, the measured hardness of the HVOF coating was 789 ± 54 $HV_{0.1}$, while the hardness of the laser remelted HVOF coating was 914 ± 17 $HV_{0.1}$.

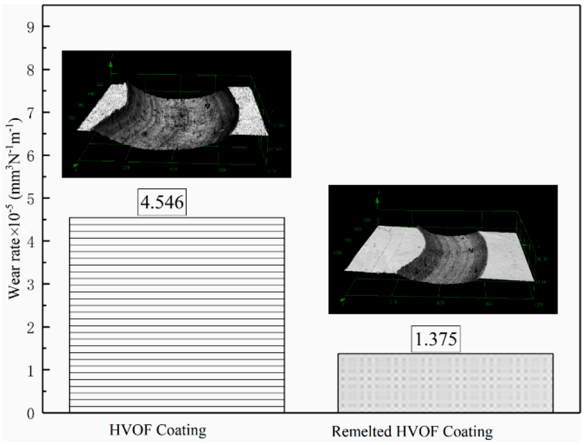

Figure 6. Wear rate and confocal scanning laser microscope (CSLM) micrographs of the coatings.

The surface morphologies of the wear tracks of the as-sprayed and laser remelted HVOF coatings are shown in Figure 7. The grooves are observed obviously on the wear track in both of the coatings. In addition, the debris caused by wear is also recognized. These indicate that the abrasion wear is the main wear mechanism for the laser remelted HVOF coating. The large difference in the hardness between the coatings and counter body caused the abrasion wear. The hardness of Al_2O_3 counter body amounts to 2055 $HV_{0.1}$ [31], which is much higher than the coatings. The harder Al_2O_3 ball could easily cut the coatings. During the test, the coatings endured high contact pressure and then caused local plastic deformation. Moreover, on the wear track surface of the HVOF coating, splat delamination is observed, which is not observed on laser remelted HVOF coating.

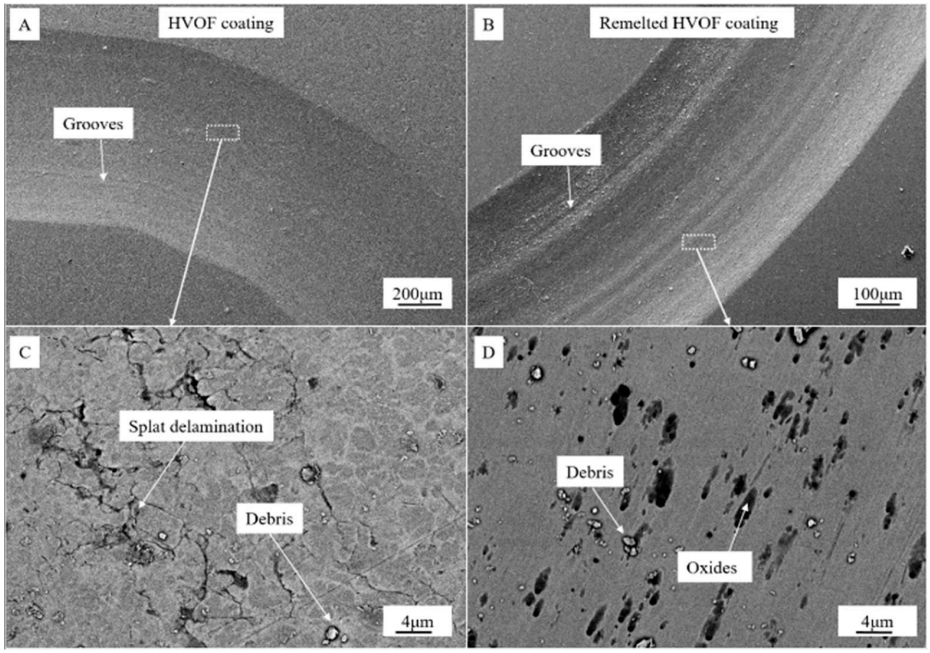

Figure 7. Surface morphologies of friction samples of the HVOF coating and the laser remelted HVOF coating.

Figure 8 shows the cross-sections of the wear tracks of the HVOF coating and the laser remelted HVOF coating. In the polished cross-section of the HVOF coating, severe splat delamination can be observed, indicating that fatigue wear is another failure mechanism in HVOF coating [26]. Different from HVOF coating, neither splat delamination nor cracks are observed in laser remelted HVOF coating. Abrasion wear is the only wear mechanism in laser remelted HVOF coating.

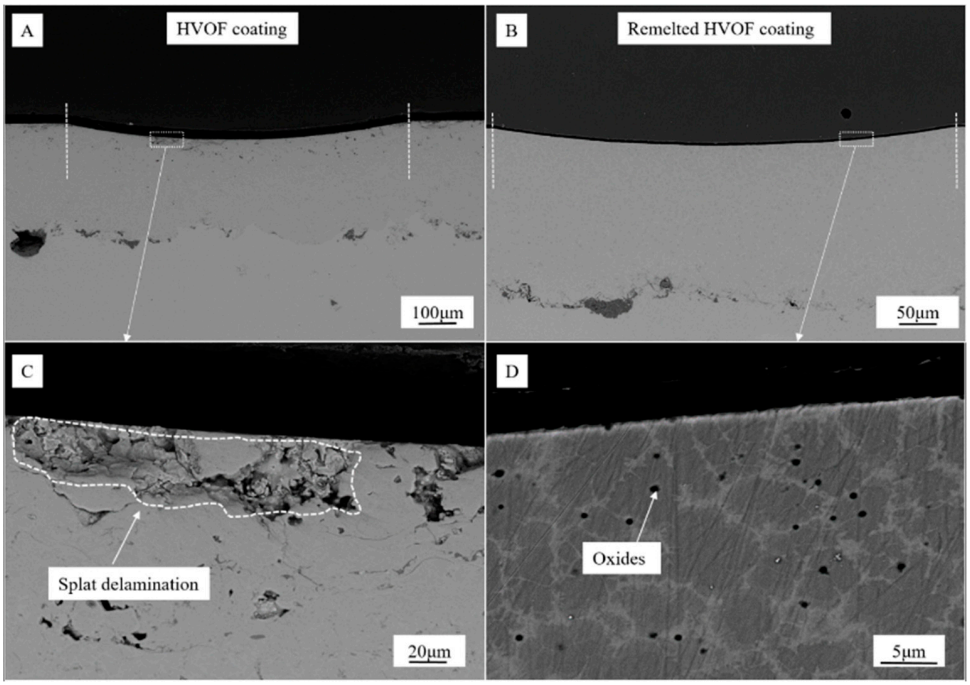

Figure 8. Cross-section views of friction samples of the HVOF coating and the laser remelted HVOF coating.

4. Conclusions

The microstructure of the laser remelted $FeCrCoNiTiAl_{0.6}$ high entropy alloy HVOF coating and the wear behavior have been investigated in this study. The following conclusions can be made:

(1) The as-sprayed $FeCrCoNiTiAl_{0.6}$ HVOF coating exhibited two separate BCC phases and aluminum oxide precipitated after laser remelting process. The laser remelted HVOF coating possessed a compact microstructure and the pre-existing pores and micro-cracks were remarkably eliminated.

(2) The laser remelted $FeCrCoNiTiAl_{0.6}$ HVOF coating had a higher microhardness of 914 ± 17 $HV_{0.1}$ and better wear resistance than HVOF coating.

(3) The major wear mechanism of the $FeCrCoNiTiAl_{0.6}$ HVOF coating and the laser remelted HVOF coating is abrasion. Fatigue wear participated in the HVOF coating.

Author Contributions: Methodology, L.C. and D.H.; software, L.L.; validation, B.H., Z.G. and L.Z.; formal analysis, Z.T.; investigation, L.C. and X.W.; data curation, L.C.; writing—original draft preparation, L.C.; writing—review and editing, Z.Z.; supervision, D.H. and Z.Z.; funding acquisition, L.C. and Z.Z. All authors have read and agreed to the published version of the manuscript.

Funding: This research was funded by the National Key R&D Program of China, grant number 2017YFB0306100; the Academy of Sciences Project of Guangdong Province, grant number 2016GDASRC-0105; the GDAS' Project of Science and Technology Development, grant number 2021GDASYL-20210103092, 2017GDASCX-0115 and 2018GDASCX-0115. The APC was funded by the Academy of Sciences Project of Guangdong Province.

Conflicts of Interest: The authors declare no conflict of interest.

References

1. Cantor, B.; Chang, I.T.H.; Knight, P.; Vincent, A.J.B. Microstructural development in equiatomic multicomponent alloys. *Mater. Sci. Eng. A* **2004**, *375–377*, 213–218. [CrossRef]
2. Chen, T.K.; Shun, T.T.; Yeh, J.W.; Wong, M.S. Nanostructured nitride films of multi-element high-entropy alloys by reactive DC sputtering. *Surf. Coat. Technol.* **2004**, *188–189*, 193–200. [CrossRef]
3. Hsu, C.-Y.; Yeh, J.-W.; Chen, S.-K.; Shun, T.-T. Wear resistance and high-temperature compression strength of Fcc CuCoNiCrAl0.5Fe alloy with boron addition. *Metall. Mat. Trans. A* **2004**, *35*, 1465–1469. [CrossRef]
4. Huang, P.-K.; Yeh, J.-W.; Shun, T.-T.; Chen, S.-K. Multi-Principal-Element Alloys with Improved Oxidation and Wear Resistance for Thermal Spray Coating. *Adv. Eng. Mater.* **2004**, *6*, 74–78. [CrossRef]
5. Yeh, J.-W.; Chen, S.-K.; Lin, S.-J.; Gan, J.-Y.; Chin, T.-S.; Shun, T.-T.; Tsau, C.-H.; Chang, S.-Y. Nanostructured High-Entropy Alloys with Multiple Principal Elements: Novel Alloy Design Concepts and Outcomes. *Adv. Eng. Mater.* **2004**, *6*, 299–303. [CrossRef]
6. Yeh, J.-W.; Lin, S.-J.; Chin, T.-S.; Gan, J.-Y.; Chen, S.-K.; Shun, T.-T.; Tsau, C.-H.; Chou, S.-Y. Formation of simple crystal structures in Cu-Co-Ni-Cr-Al-Fe-Ti-V alloys with multiprincipal metallic elements. *Metall. Mat. Trans. A* **2004**, *35*, 2533–2536. [CrossRef]
7. Chen, L.; Zhou, Z.; Tan, Z.; He, D.; Bobzin, K.; Zhao, L.; Öte, M.; Königstein, T. High temperature oxidation behavior of $Al_{0.6}CrFeCoNi$ and $Al_{0.6}CrFeCoNiSi_{0.3}$ high entropy alloys. *J. Alloys Compd.* **2018**, *764*, 845–852. [CrossRef]
8. Chang, S.-Y.; Li, C.-E.; Huang, Y.-C.; Hsu, H.-F.; Yeh, J.-W.; Lin, S.-J. Structural and thermodynamic factors of suppressed interdiffusion kinetics in multi-component high-entropy materials. *Sci. Rep.* **2014**, *4*, 4162. [CrossRef]
9. Hobbs, R.A.; Tin, S.; Rae, C.M.F. A castability model based on elemental solid-liquid partitioning in advanced nickel-base single-crystal superalloys. *Metall. Mat. Trans. A* **2005**, *36*, 2761–2773. [CrossRef]
10. Reed, R.C.; Tao, T.; Warnken, N. Alloys-By-Design: Application to nickel-based single crystal superalloys. *Acta Mater.* **2009**, *57*, 5898–5913. [CrossRef]
11. Senkov, O.N.; Senkova, S.V.; Woodward, C. Effect of aluminum on the microstructure and properties of two refractory high-entropy alloys. *Acta Mater.* **2014**, *68*, 214–228. [CrossRef]
12. Wu, W.-H.; Yang, C.-C.; Yeh, J.-W. Industrial development of high-entropy alloys. *Ann. Chim. Sci. Mat.* **2006**, *31*, 737–747. [CrossRef]
13. Yeh, A.-C.; Chang, Y.-J.; Tsai, C.-W.; Wang, Y.-C.; Yeh, J.-W.; Kuo, C.-M. On the Solidification and Phase Stability of a Co-Cr-Fe-Ni-Ti High-Entropy Alloy. *Metall. Mat. Trans. A* **2014**, *45*, 184–190. [CrossRef]
14. Zhu, J.M.; Fu, H.M.; Zhang, H.F.; Wang, A.M.; Li, H.; Hu, Z.Q. Microstructure and compressive properties of multiprincipal component AlCoCrFeNiCx alloys. *J. Alloys Compd.* **2011**, *509*, 3476–3480. [CrossRef]
15. Weng, F.; Chew, Y.; Zhu, Z.; Yao, X.; Wang, L.; Ng, F.L.; Liu, S.; Bi, G. Excellent combination of strength and ductility of CoCrNi medium entropy alloy fabricated by laser aided additive manufacturing. *Addit. Manuf.* **2020**, *34*, 101202.
16. Chew, Y.; Bi, G.; Zhu, Z.G.; Ng, F.L.; Weng, F.; Liu, S.B.; Nai, S.M.L.; Lee, B.Y. Microstructure and enhanced strength of laser aided additive manufactured CoCrFeNiMn high entropy alloy. *Mater. Sci. Eng. A* **2019**, *744*, 137–144. [CrossRef]
17. Bi, G.; Chew, Y.; Weng, F.; Zhu, Z.; Ng, F.L.; Lee, B.Y. Process study and characterization of properties of FerCrNiMnCo high-entropy alloys fabricated by laser-aided additive manufacturing. *Adv. Laser Process. Manuf. II* **2018**, *10813*, 1–10.
18. Hsu, W.-L.; Murakami, H.; Yeh, J.-W.; Yeh, A.-C.; Shimoda, K. On the study of thermal-sprayed $Ni_{0.2}Co_{0.6}Fe_{0.2}CrSi_{0.2}AlTi_{0.2}$ HEA overlay coating. *Surf. Coat. Technol.* **2017**, *316*, 71–74. [CrossRef]
19. Li, T.; Liu, Y.; Liu, B.; Guo, W.; Xu, L. Microstructure and Wear Behavior of $FeCoCrNiMo_{0.2}$ High Entropy Coatings Prepared by Air Plasma Spray and the High Velocity Oxy-Fuel Spray Processes. *Coatings* **2017**, *7*, 151. [CrossRef]
20. Löbel, M.; Lindner, T.; Kohrt, C.; Lampke, T. Processing of AlCoCrFeNiTi high entropy alloy by atmospheric plasma spraying. *IOP Conf. Ser. Mater. Sci. Eng.* **2017**, *181*, 12015. [CrossRef]
21. Tian, L.-H.; Xiong, W.; Liu, C.; Lu, S.; Fu, M. Microstructure and Wear Behavior of Atmospheric Plasma-Sprayed AlCoCrFeNiTi High-Entropy Alloy Coating. *J. Mater. Eng. Perform.* **2016**, *25*, 5513–5521. [CrossRef]

22. Wang, L.M.; Chen, C.C.; Yeh, J.W.; Ke, S.T. The microstructure and strengthening mechanism of thermal spray coating $Nix Co_{0.6} Fe_{0.2} Cry Siz Al Ti_{0.2}$ high-entropy alloys. *Mater. Chem. Phys.* **2011**, *126*, 880–885. [CrossRef]
23. Löbel, M.; Lindner, T.; Mehner, T. Microstructure and Wear Resistance of AlCoCrFeNiTi High-Entropy Alloy Coatings Produced by HVOF. *Coatings* **2017**, *7*, 144. [CrossRef]
24. Cai, Z.; Cui, X.; Liu, Z.; Li, Y.; Dong, M.; Jin, G. Microstructure and wear resistance of laser cladded Ni-Cr-Co-Ti-V high-entropy alloy coating after laser remelting processing. *Opt. Laser Technol.* **2018**, *99*, 276–281. [CrossRef]
25. Jiang, L.; Zhou, G. Facile synthesis of monodispersed nanocrystalline anatase TiO_2 particles with large surface area and enhanced photocatalytic activity for degradation of organic contaminant in wastewaters. *Mater. Sci. Semicond. Process.* **2012**, *15*, 108–111. [CrossRef]
26. Chen, L.; Bobzin, K.; Zhou, Z.; Zhao, L.; Öte, M.; Königstein, T.; Tan, Z.; He, D. Wear behavior of HVOF-sprayed $Al_{0.6}$TiCrFeCoNi high entropy alloy coatings at different temperatures. *Surf. Coat. Technol.* **2019**, *358*, 215–222. [CrossRef]
27. Pawlowski, L.; Smurov, I. Modeling of high power laser interaction with APS deposited FeCrTiC. *Surf. Coat. Technol.* **2002**, *151–152*, 308–315. [CrossRef]
28. Zhou, Z.; Wang, L.; Wang, F.C.; Zhang, H.F.; Liu, Y.B.; Xu, S.H. Formation and corrosion behavior of Fe-based amorphous metallic coatings by HVOF thermal spraying. *Surf. Coat. Technol.* **2009**, *204*, 563–570. [CrossRef]
29. Yue, T.; Xie, H.; Lin, X.; Yang, H.; Meng, G. Microstructure of Laser Re-Melted AlCoCrCuFeNi High Entropy Alloy Coatings Produced by Plasma Spraying. *Entropy* **2013**, *15*, 2833–2845. [CrossRef]
30. Zhou, Y.J.; Zhang, Y.; Kim, T.N.; Chen, G.L. Microstructure characterizations and strengthening mechanism of multi-principal component $AlCoCrFeNiTi_{0.5}$ solid solution alloy with excellent mechanical properties. *Mater. Lett.* **2008**, *62*, 2673–2676. [CrossRef]
31. Zhang, Z.; Li, X.; Almandoz, E.; Fuentes, G.G.; Dong, H. Sliding friction and wear behaviour of Titanium-Zirconium-Molybdenum (TZM) alloy against Al_2O_3 and Si_3N_4 balls under several environments and temperatures. *Tribol. Int.* **2017**, *110*, 348–357. [CrossRef]